Journal of Sol-Gel Science and Technology (2023) 106:816–826
https://doi.org/10.1007/s10971-023-06092-z

ORIGINAL PAPER: SOL-GEL AND HYBRID MATERIALS FOR ENERGY, ENVIRONMENT AND BUILDING APPLICATIONS

Zirconia-based coatings for the protection of ferritic-martensitic steels in a molten salt environment for CSP technology

Víctor Encinas-Sánchez[1] · Antonio Macías-García[2] · Gustavo García-Martín[1] · Francisco Javier Pérez Trujillo[1] · Jesús Manuel Rodríguez-Rego[2]

Received: 24 November 2022 / Accepted: 13 March 2023 / Published online: 8 April 2023

Abstract

The ferritic-martensitic 9Cr-1Mo steel was coated with a sol-gel ZrO2-3%molY2O3 solution by dip-coating. The protective properties of the coating were evaluated in contact with Solar Salt for CSP applications. The coated and uncoated steels were tested at 500 °C in contact with the Solar Salt for 2000 h. Gravimetric, microstructural and compositional studies were performed to compare their behaviour, against corrosion. Results revealed the beneficial influence of the coating on the corrosion resistance of P91 in contact with molten nitrate salt. Weight gain of the coated samples remained practically unaltered throughout the test, while the uncoated samples showed a weight increase with the formation of multi-layered, non-adherent corrosion layers that were spalled during the test. The microstructural and compositional study performed on the samples shows the maintenance of the coating layer and the presence of a 5.18 µm-thick diffusion layer primarily composed of Fe-Zr species, which reduce the ionic diffusion and improve the protective properties. Results reveal the possible suitability of the proposed system as a potential solution to the severe corrosion problems industrial tanks and pipes in contact with Solar Salt.

Graphical Abstract

The coating of 9Cr-1Mo ferritic-martensitic steel with a sol-gel solution of ZrO_2 3% mol Y_2O_3 achieved a substantial improvement avoiding corrosion problems and postulating the proposed system as a potential solution to the severe corrosion problems of industrial tanks and pipes in contact with solar salt.

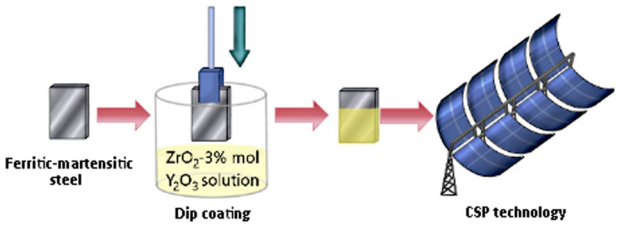

Keywords Coatings · Molten salt · Ferritic-martensitic steel · Corrosion · CSP

✉ Jesús Manuel Rodríguez-Rego
jesusrodriguezrego@unex.es

[1] Surface Engineering and Nanostructured Materials Research Group, Complutense University of Madrid, Complutense Avenue s/n, Madrid, Spain

[2] Department of Mechanical, Energetic and Materials Engineering School of Industrial Engineering, Universidad de Extremadura, Avda. de Elvas, s/n, 06006 Badajoz, Spain

Highlights

- The proposed coatings achieved that the samples remained unchanged in weight, indicating the stability of the system.
- The uncoated samples showed spallation of oxide scale and corrosion products.
- The coated samples retained the coating layer and the presence of a diffusion layer composed of Fe–Zr species.
- Ø The above results show the suitability of the system for applications where there are corrosion problems due to contact with solar salt.

1 Introduction

Interest in molten salts as heat transfer fluids and thermal storage media in concentrated solar power (CSP) plants has increased [1]. One of the most commonly used salts in CSP is molten nitrate salts in heat transfer and storage applications. Salt based on alkaline nitrates (Solar Salt, 60 wt.% NaNO3/40 wt.% KNO3) is the most used medium [2]. This salt is characterized by high density, high specific heat, low melting point, high thermal stability, low viscosity in its molten state, and low vapor pressure [3, 4], as well as a competitive price [1]. However, according to several experiences with this fluid in CSP environments, solar salt can cause significant corrosion in the steel components of the power plant [5]. This fact is closely related to the nitrite, chloride and sulfate impurities contained in industrial grade salt formulations [1, 6] and also with the high operating temperature and chemical properties of the salt itself [7, 8]. Corrosion degradation of materials by molten salts in CSP plants is under study [5]. Ferritic-martensitic steels have been used for industrial applications due to their cost, despite having worse properties than other materials, such as stainless steel, as they are prone to localized corrosion under severe conditions [9, 10]. One of the methods used to avoid this phenomenon is protective coatings [11]. The use of high temperature corrosion resistant coatings on ferritic-martensitic steels would be an important advance for this type of material. This solution not only would help to overcome the corrosion problems of using ferritic-martensitic steels at these temperatures, but also would allow the CSP industry to improve the LCOE (Levelised Cost of Energy) by reducing O&M (Operating and Maintenance) costs [12]. At present, results on the effect of protective coatings on steels against corrosion caused by molten nitrate salts are very limited. Some results are related to the effect of aluminising [13, 14] and multilayer coatings based on nickel and aluminium [15]. Dorcheh and Galetz [14] proposed aluminium slurries as a solution for the corrosion process suffered by P91 and 304 steels in molten nitrates. They performed isothermal corrosion tests at 600 °C under flowing laboratory air for up to 2500 h. Their results were promising and they concluded that the coating needed to be optimised to improve its behaviour under cyclic conditions. To protect low-alloy steels against corrosion caused by molten solar salts, the multilayer PVD NiV-Al metallic coating has been used, resulting in a significant reduction of corrosion rates and an improvement in the durability of the developed coatings and the underlying steel substrate [15]. Audigié et al. [16] also proposed slurry aluminide coatings deposited on ferritic-martensitic P92 steel, performing isothermal tests at 550 °C and 580 °C for 2000 h. These authors obtained promising results and observed the formation of numerous protective FeAl species in the outer layers of the coated substrates. Fähsing et al. [17] to improve the molten salt corrosion resistance of VM12 and T91 ferritic-martensitic steels proposed the use of Cr diffusion coatings and Al-Si slurry coatings. These authors carried out corrosion tests on molten nitrates with different Cl^- and SO_4^{2-} contents at 560 °C for 1000 h and obtained promising results, although longer exposure times are required to confirm their suitability. Other authors have studied the use of protective coatings on steels that operate in contact with molten carbonates and chlorides. In this respect, Gómez-Vidal and Morton [18] assessed the employment of SiO_2 coatings on SS347 working in contact with eutectic mixtures of carbonates and chlorides (K_2CO_3-Na_2CO_3, K_2CO_3-Na_2CO_3-Li_2CO_3, NaCl-LiCl and NaCl-KCl) at temperatures that ranged between 600 °C and 750 °C. These types of coatings were able to protect the substrate during short-term tests, but longer tests are needed to evaluate the chemical stability of the system.

A variety of techniques are used for the deposition of coatings, such as chemical vapor deposition (CVD), physical vapour deposition (PVD), electrochemical deposition, plasma spraying and the sol-gel process [19]. Among these, sol-gel coatings present numerous advantages, several of the most important being [19, 20]: they generally present low processing temperature; they may be deposited on complex shapes and can be produced without the need for machining or melting; and finally, they are formed by 'green' coating technologies, i.e., the compounds used do not introduce impurities into the end product as initial substances. One of the most commonly used sol-gel protective coatings is formed by oxides, such as TiO2 [21], ZrO2 [22], SiO2-ZrO2 [23] and ZrO2-CeO2 [24]. Within these, yttrium-stabilised zirconia seems to be a great option owing to its properties [25]. Moreover, sol-gel solutions can be deposited by: spin coating, sputter coating, electrodeposition, dip coating, etc. [26, 27]. The dip coating technique allows the preparation of uniform

coatings by simply controlling the removal rate and has a low cost [28]. Sol-gel coatings offer advantages, such as [19, 20]: low processing temperature; they allow deposition on complex shapes, can be produced without machining or casting… etc. Sol-gel protective coatings formed by oxides, such as TiO_2 [21], ZrO_2 [22], SiO_2-ZrO_2 [23] and ZrO_2-CeO_2 are widely used [24]. Within these, yttria-stabilized zirconia seems to be a great choice due to its properties [25].

In this study, zirconium-based coatings dip-deposited on P91 and uncoated P91 substrate were tested in contact with molten nitrate salts at 500 °C up to 2000 h, and the results obtained for coating resistance were compared.. Finally, the coatings were tested up to failure, and the locations were analyzed from the morphological and compositional point of view.

2 Materials and methods

2.1 Materials

2.1.1 Steel samples

The substrate used was 9Cr-1Mo ferritic-martensitic steel (ASME Grade P91/T91), one of the most widely used steels in engineering. P91 due to its high LCF life, could have a great interest in its application in high temperature systems [29]. P91 contains a higher percentage of Cr (~9%) and a composition, of 0.10% C, 0.25% Si, 0.40% Mn, 9.00% Cr, 0.95% Mo, 0.20% V, 0.07% Nb, and 0.04% N in weight percentage. The substrates were fabricated with a size of $20 \times 10 \times 2\ mm^3$ and were surface polished

2.1.2 Manufacture of the sol–gel solution

The yttria-doped zirconium sol-gel solution was prepared by mixing a solution of N-propoxide/1-propanol/H_2O/HNO_3 with a solution of yttrium acetate/2-propanol/H_2O/HNO_3 both with a molar ratio of 1/15/6/1. The mixture was mechanically stirred for 30 min, and then finished by adding H2O followed by mechanical stirring for 1 h [30].

2.2 Coating deposition and characterisation

The materials in sol phase, before gelation, were used to coat P91 samples 20 mm long, 10 mm wide and 1.5 mm thick using a KSV-Nima dip coater. Before starting the coating process, the substrates were ground and polished (with sandpaper, up to 800 grains cm^{-2} and polishing cloths up to 3 μm), and ultrasonically cleaned with acetone and deionised water, for 5 min. To dip-coat the samples, a withdrawal speed of the substrate equal to 25 mm·min^{-1} was used. The coated substrates were dried at 100 °C, 60 min and subsequently sintered at 500 °C, 120 min, with a heating and cooling velocity of 3 °C min−1. This heat treatment promotes the densification of the film without unsuitable degradations. The surface preparation, withdrawal rate and heat treatment were selected on the basis of previously published studies [30, 31], owing to the good thickness uniformity they provide.

The coated substrates were then evaluated by weight difference and characterized by scanning electron microscopy (SEM) with a JEOL® JSM-820 equipment and by X-ray diffraction (XRD) with a PANalytical® equipment (model X′Pert PRO MRD). The SEM allows to study of morphology and chemical composition of the surface and corroded samples after the isothermal immersion test. In the SEM of the cross sections of the samples, these were mounted on a phenolic resin (Buehler ®) and ground with 240, 320, 400, 600, 1000, 2400, and 4000 silicon carbide with distilled water. XRD allows phase analysis of the coating layer deposited on the samples. The XRD patterns obtained were compared with the standards compiled by the Joint Committee on Powder Diffraction and Standards (JCPDS) to identify the phases.

2.3 Preparation and characterisation of the salt mixture

Solar salt (60 wt% $NaNO_3$/40 wt% KNO_3) was used as a corrosive agent, employed in solar power plants [32]. The eutectic $NaNO_3$/KNO_3 was prepared from the above compounds (purity >99%) supplied by BASF® and Haifa® respectively. From the starting salts, the impurity level of the prepared mixture was of 130 ppm Cl^- and 60 ppm SO_4^{2-}. The impurity level is a parameter that highly influences the properties and corrosive action of the salt (the higher the impurities, the higher the corrosive behaviour) [6].

The presence of impurities in the prepared binary salt influences its melting point and decomposition temperature. The melting point of the salt was determined by differential scanning calorimetry (DSC) with a DSC-Q20 calorimeter using a hermetically closed aluminum crucible and the thermal stability was measured by thermogravimetric analysis (TGA) with a SDT-Q600 equipment using an open platinum crucible. In both crucibles, 10 mg of sample were used in each case, in an inert nitrogen atmosphere of 50 ml·m^{-1} and at a heating velocity of 10 °C-min^{-1}. Before the analysis, both instruments were calibrated with indium.

2.4 Corrosion study of the coated samples

Isothermal immersion tests were carried out by the gravimetric method. The coated and uncoated samples were

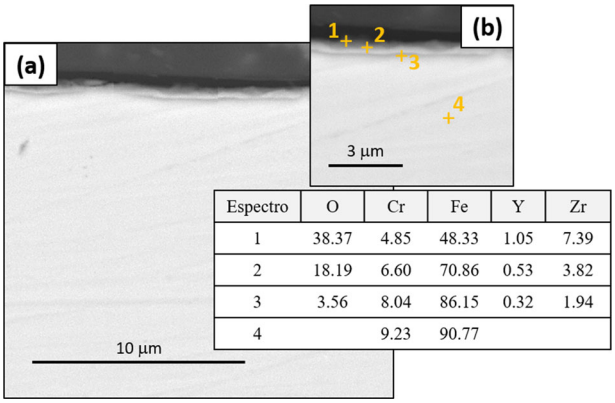

Espectro	O	Cr	Fe	Y	Zr
1	38.37	4.85	48.33	1.05	7.39
2	18.19	6.60	70.86	0.53	3.82
3	3.56	8.04	86.15	0.32	1.94
4		9.23	90.77		

Fig. 1 Cross-section SEM micrographs and EDX analysis (in atomic percentage) of the coated P91 specimens before testing: (**a**) x500; (**b**) x10000

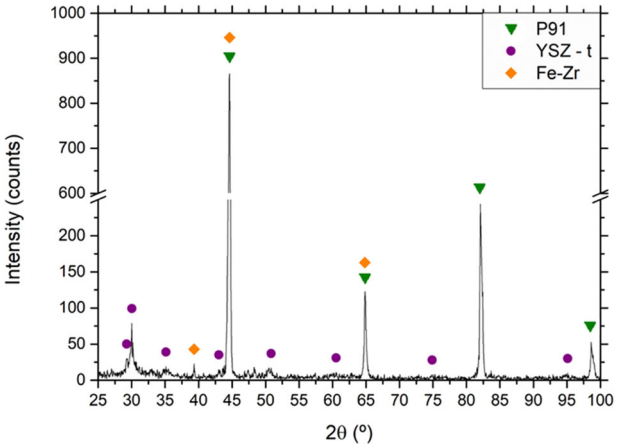

Fig. 2 XRD analysis of the coated samples before testing

immersed in 50 ml of the molten salt to a depth of about 3.5 cm in alumina crucibles.

The crucibles together with the solid salt mixture were placed inside an electrical chamber (Carbolite®) until the required temperature was reached in an air atmosphere. The corrosion temperature assay was selected on the basis of previous TGA results. Samples immersed in the molten salt were weighed at 0, 24, 48, 72, 72, 168, 250, 500, 750, 1000, 1250, 1500, 1750 and 2000 h. Three samples were extracted from each system analyzed (P91 coated and P91 uncoated) for each working time, cooled slowly and rinsed with hot distilled water to remove salt residues. Subsequently, they were dried and weighed (average of five weight values). The formula (Eq. 1) used to calculate the mass increase with time is.

$$\frac{\Delta m}{S_0} = \frac{m_f - m_i}{S_0} \tag{1}$$

where m_i is the initial mass of the specimen, m_f is the mass of the sample at the selected time and S_0 is the initial area of the specimen.

After 2000 h of testing, three samples from each system were extracted from the binary salt for examination and microstructural analysis, as described in Section 2.2.

3 Results and discussion

3.1 Characterisation of the coated samples

To acquire the surface morphologies and the phases formed, coatings prepared under the conditions described in Section 2.2 were subjected to SEM-EDX and XRD. Figure 1a, shows that the morphology of the ZrO2-Y2O3 coating is uniform and homogeneous, with a thickness of 463 nm. As previously reported [33], the coating grows by forming coral-like agglomerations that are embedded within trenches, while a diffusion zone, with a depth of ~315 nm, appears as consequence of the thermal treatment to which the coatings are subjected. This diffusion zone was also confirmed by a compositional analysis carried out using energy-dispersive X-ray spectrometry (EDX) (see Fig. 1b). The EDX analysis showed the higher atomic percentage of Zr, Y and O in the upper layer (Spectrum 1: 7.39%, 1.05%, and 38.37%, respectively), which corresponds properly to the deposited coating, and its gradual reduction as you go deeper into the sample (Spectrum 3: 1.94%, 0.32% and 3.56%, respectively). The results also reveal the outer diffusion of Fe (48.33 % in Spectrum 1), which possibly indicates the presence of Zr-Fe species.

Figure 2 shows the XRD analysis of the coatings deposited on P91 steel. XRD results suggest the presence of a tetragonal phase as the main phase responsible for the properties of the system [34]. Additionally, the analysis reveals the presence of Fe-Zr peaks, which correspond to the species formed in the previously identified diffusion layer. Carrasco-Amador [35] and Chęcmanowski [36] also suggested the formation of these kinds of species, which improve the protective properties of the coated system [37].

It is important to highlight that unlike the results reported in [33], the coated samples in this study presented a high uniformity and homogeneity, which as previously reported in [30] clearly indicates the importance of the substrate surface preparation (polishing vs roughing).

3.2 Characterisation of the salt mixture

As described above, the impurity level is a parameter that highly influences the properties of the salt [6]. This is why the melting point and decomposition temperature of the prepared salt were determined by DSC and TGA, respectively. These parameters helped determine the heat treatment to which the salt would be subjected, and mainly to

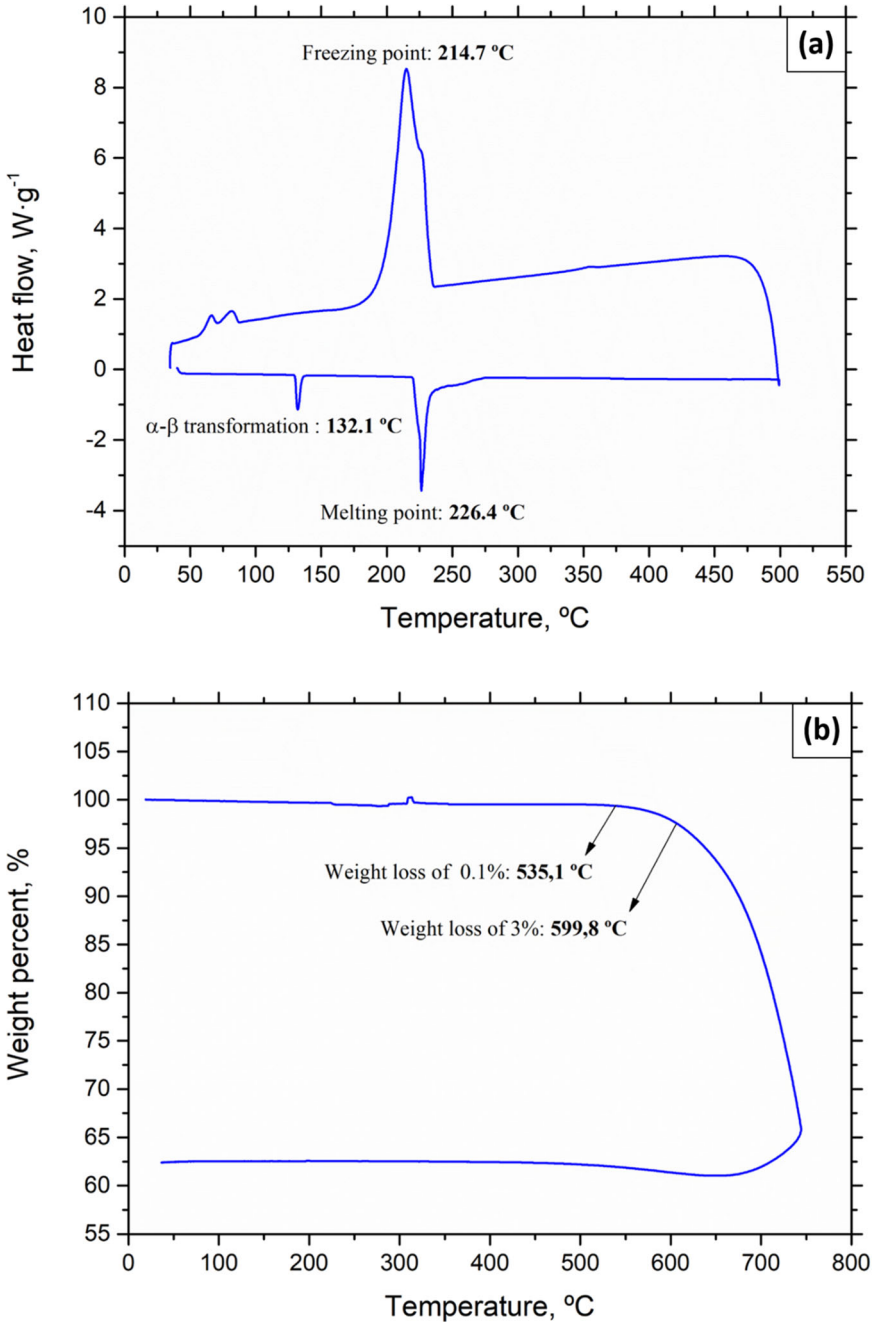

Fig. 3 Characterisation of the prepared salt mixture: (**a**) calorimetric curve; and (**b**) thermogravimetric curve

select the temperature of the corrosion tests. This temperature corresponded to the maximum working temperature of the salt.

Thus, Fig. 3a shows the curve obtained by DSC, where three peaks are detected. The first of the peaks (132.1 °C) corresponds to the α–β transformation [38]. The second represents the melting point of the salt mixture, 226.4 °C, while the peak appearing at 214.7 °C during the cooling stage corresponds to the freezing point of the salt. Figure 3b shows the results of the thermogravimetric study, in which the temperature of maximum stability corresponds to the temperature at which the weight loss of the salt mixture is first detected. That is, the sample started to degrade at 535.1 °C (weight loss percentage around 0.1%), [39]. The maximum operating temperature of the Solar Salt® is 565 °C [40], and a percentage weight loss (around 3%) [39], which explains the differences with the temperature established for this study. The temperature obtained at this percentage of weight loss for the tested salt was also shown in Fig. 1, being 599.8 °C, similar to that obtained in other studies [39]. These differences in the maximum operating temperature of Solar Salt® are attributable to the presence of impurities [41]. Therefore, the binary salt prepared is stable at 500 °C, the temperature selected for the corrosion tests.

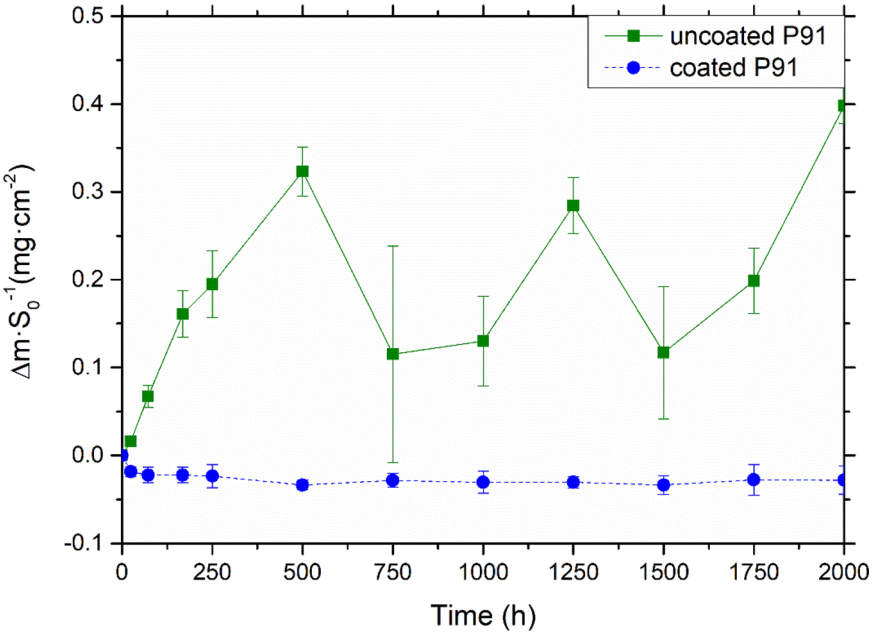

Fig. 4 Gravimetric results for uncoated and coated P91 specimens immersed in Solar Salt at 500 °C

3.3 Corrosion study of the samples

3.3.1 Gravimetric analysis

During the corrosion test, gravimetric analysis of the samples was carried out. For this purpose, the weight of the samples introduced into the molten salt mixture for 0, 24, 48, 72, 168, 250, 250, 500, 750, 10 100, 1250, 1500, 1750, and 2000 h was determined.

Figure 4 represents the variation of the gravimetric mass with time in the P91 coated and uncoated samples immersed in the molten nitrate salt at 500 °C. The results correspond to the weight of the specimens after cleaning with water and drying. The figure shows that P91 in contact with the molten nitrate salt increases its weight as reported by other authors [14, 17, 42]. The weight gain value showed increases and decreases, which seems to indicate the existence of detachments along the test.

The weight change curve of the samples reveals that uncoated P91 does not show a protective action in contact with molten nitrate salts, since the oxide flakes formed on its surface are prone to buckling and blistering [14]. While the coated P91 specimens have higher corrosion resistance (3. 5 times less mass increase than uncoated P91), after 500 h of testing. After 1000 h of testing, the difference in weight gained between the coated and uncoated samples is smaller (coated P91 shows 1.75 times less mass gain than uncoated P91). These weight losses are a consequence of the detachment of non-adherent corrosion layers and were also observed by other authors [42]. At the end of the test, the uncoated P91 sample achieves an average weight gain of 0.3980 mg·cm^{-2} and the coated sample with a mean weight loss of 0.0280 mg·cm^{-2}

Likewise, the weight change curves also show that up to 72 h there is an initial mass loss in the coated P91 (see Fig. 4). This mass loss may be due to a partial dissolution of some coating components in molten nitrate salts during the initial period of the test. Between 72 h and 2000 h of testing the weight gain of the coated steel remains practically unaltered, which indicates the stability of the system during the test. Agüero et al. [43] also found an initial mass loss in slurry aluminide coatings, this being attributed to undiffused slurry residues ('bisque').

3.3.2 Metallographic and composition investigations

Scanning Electron Microscopy coupled with EDX (SEM-EDX) for elemental analysis was performed in order to characterise the sample at high resolution. Furthermore, XRD analyses were carried out to compositionally identify the tested samples.

3.3.2.1 Uncoated samples The spallation of oxide scales and corrosion products in the uncoated P91 samples, to which the mass losses observed in the gravimetric analysis are attributed, was also observed by SEM. As Fig. 5 indicates, cross-section micrographs clearly show the formation of non-adherent corrosion layers, these leading to the above-mentioned spallation, which, as stated by Audigié et al. [42], occurs randomly throughout the entire test. This randomness in the spallation process makes it difficult to compare the obtained results with those obtained by other authors.

EDX analysis makes it possible to clearly identify the multi-layered structure of these non-adherent corrosion

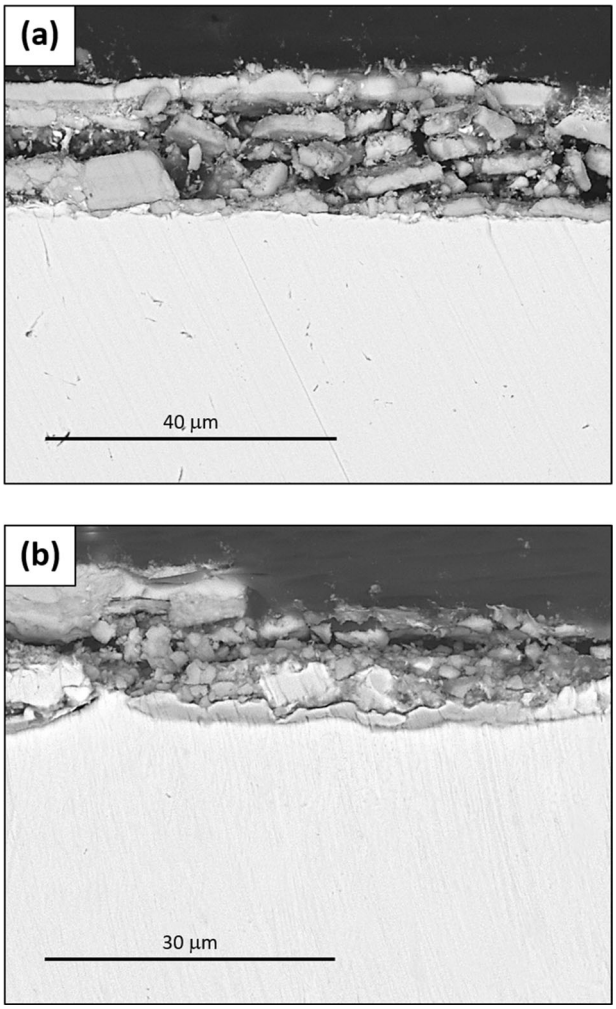

Fig. 5 Cross-section micrographs of uncoated P91 specimens after 2000 h in contact with Solar Salt at 500 °C using a back-scattered electron detector at various magnifications: (**a**) x1500; and (**b**) x2000

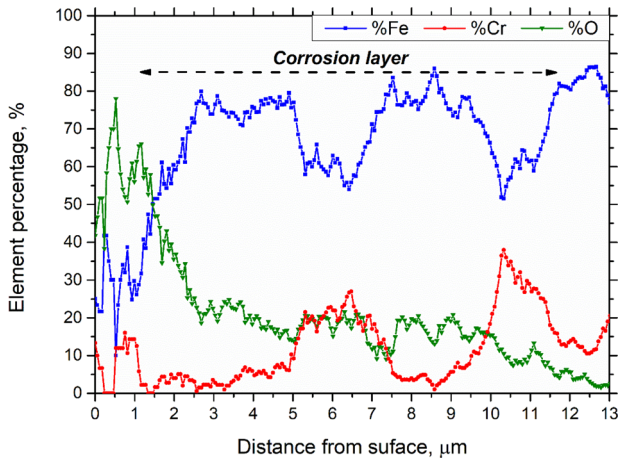

Fig. 6 Lineal cross-section EDX analysis of the uncoated P91 specimens after 2000 h in contact with Solar Salt at 500 °C

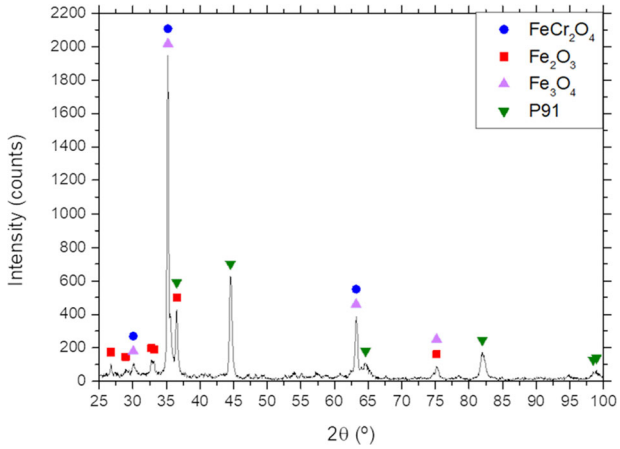

Fig. 7 XRD analysis of the uncoated P91 specimens after 2000 h in contact with Solar Salt at 500 °C

layers and their elemental composition. As shown in Fig. 6, the corrosion layers are composed by iron oxides on the outer side and iron-chromium spinels on the inner side. XRD analysis confirmed the elemental composition of these corrosion products, consisting of Fe_2O_3 and Fe_3O_4 in outer layer and $FeCr_2O_4$ in the inner layer (see Fig. 7). The iron oxides that constitute the outer layer are known for their low adherence, mainly in the case of Fe_2O_3, and lower protective behaviour compared to other oxides, such as Al_2O_3 [44].

These results are in-line with those obtained by Fäshing [17], Dorcheh [14], Audigié [42] and Gurr [15], who also found these multi-layered structures at higher test temperatures (560–600 °C). However, given the difficulty of distinguishing Fe_3O_4 and $FeCr_2O_4$ phases from XRD results due to overlapping peaks, authors such as Audigié et al. [40] proved the presence of Fe_3O_4, but did not confirm the presence of $FeCr_2O_4$, attributing it to the high solubility of chromates in nitrate molten salts [45].

3.3.2.2 Coated samples Fig. 8 shows the SEM cross-section micrographs of the coated samples after 2000 h of testing. SEM micrographs show the good behaviour of the samples after being in contact with molten salt during 2000 h at 500 °C, especially when compared to uncoated samples. One aspect of particular note is the diffusion layer that emerges from the punctual EDX analyses performed on the cross-section (see Fig. 8). This seems to indicate that an inner diffusion of the coating's components into the substrate takes place. In this diffusion layer the atomic percentage of Zr decreases from 14.60% in the outer zone (see Spectrum 1 in Fig. 8) to 0.65% in the inner zone (see Spectrum 6 in Fig. 8). It is also important to highlight the outer diffusion of Fe in the system, which reaches atomic percentages of around 70% in Spectrum 2, while Cr does

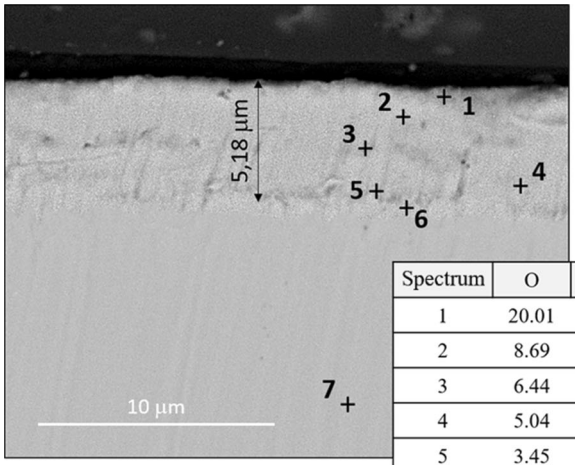

Spectrum	O	Cr	Fe	Y	Zr
1	20.01	5.95	58.46	0.98	14.60
2	8.69	7.51	71.92	0.23	11.65
3	6.44	9.04	73.81	0.13	9.58
4	5.04	9.25	80.42		5.29
5	3.45	9.85	85.89		0.82
6	1.52	10.01	87.82		0.65
7		9.21	90.79		

Fig. 8 Cross-section SEM-EDX analysis of a coated P91 specimens after 2000 h in contact with Solar Salt at 500 °C

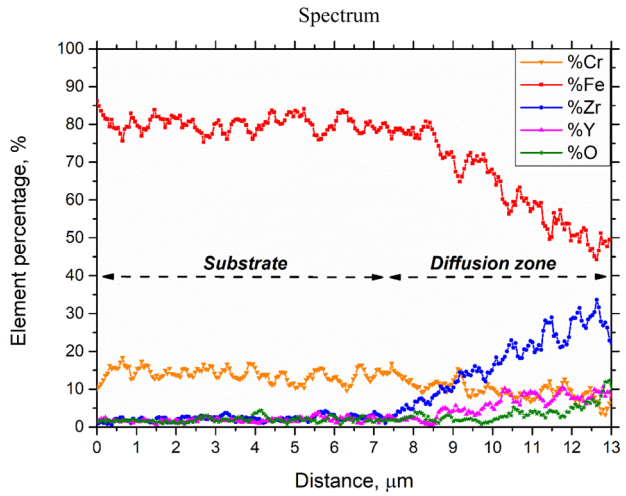

Fig. 9 Lineal cross-section EDX analysis of a coated P91 specimen after 2000 h in contact with Solar Salt at 500 °C

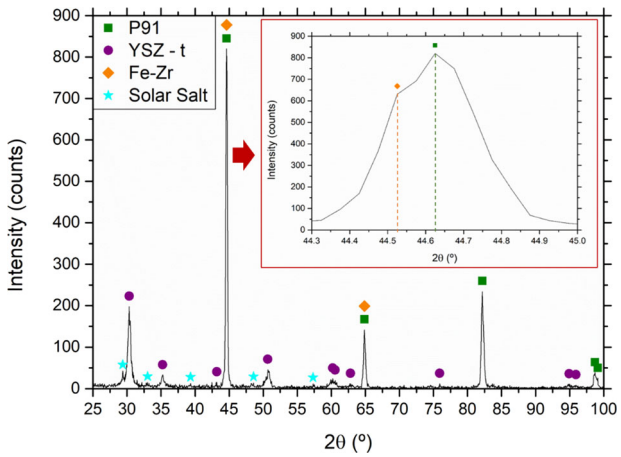

Fig. 10 XRD analysis of the coated P91 specimens after 2000 h in contact with Solar Salt at 500 °C, including the Fe-Zr and substrate peaks overlapping

not seem to play an important role. This diffusion layer can be observed more clearly in the lineal analysis performed on the same sample (see Fig. 9).

Thus, according to the EDX punctual and lineal analyses, Zr reaches a depth of about 5.18 µm. This diffusion layer can be considered as one of the main causes of the good behaviour of the coated samples. Considering the outer diffusion of Fe, the diffusion layer is essentially expected to be composed of Fe-Zr species.

Figure 10 shows the XRD analysis of the tested samples, in which the peaks corresponding to the substrate and ZrO_2-Y_2O_3 coating are identified. Additionally, species constituted by the interaction between Zr and Fe are included, which correspond to the diffusion zone previously detected by SEM-EDX. Moreover, peaks corresponding to the binary salt are detected in the analysis, which indicates the presence of salt residues on the surface of the tested samples.

As reported by Sharma [46], it is difficult to perform the identification of Fe-Zr species given the high content in Fe, since this causes the Fe-Zr peaks to overlap those corresponding to the substrate (see Fig. 10). The degree of deviation from the substrate peaks depends on the percentage of Zr, which in this particular case seems to be low (around 8–14% [46]), which is in agreement with those values obtained by EDX. These results would clearly support the presence of the diffusion layer constituted by Zr-Fe species.

Diffusion in sol-gel coatings in air atmospheres has been widely studied by several authors. Czerwinski and Szpunar [47] affirmed that CeO_2 sol-gel coatings reduce the oxidation rate in Cr_2O_3-forming steels because Ce^{4+} cations form pairs with cationic vacancies in the oxide grain boundaries, thus blocking these fast ionic paths. Baron et al. [36] also proposed that a similar mechanism occurs in sol-gel ZrO_2-Y_2O_3 coatings. These authors affirmed that in air a

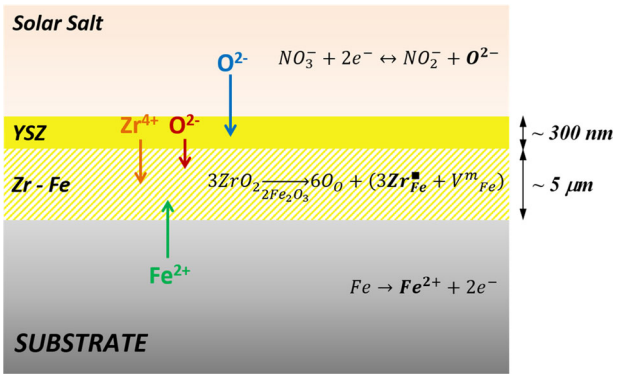

Fig. 11 Corrosion mechanism followed by a coated P91 specimen throughout a 2000-hour test in contact with Solar Salt at 500 °C

thin Fe_2O_3 layer is formed near the coating layer, which allows ZrO_2 to react with this iron oxide and form pairs with vacancies due to Coulombic

$$3ZrO_2 \underset{2Fe_2O_3}{\rightarrow} 6O_O + \left(3Zr^{\blacksquare}_{Fe} + V^{m}_{Fe}\right) \quad (2)$$

Although there is formation of a new vacancy of iron, there are three zirconia cations available to form pairs with the vacancies of iron from the oxide. Consequently, the mobile vacancy concentration in the oxide decreases due to the formation of such pairs. Once this protective scale is formed, the ionic diffusion is slowed, decreasing the oxidation rate [36]. Chęcmanowski and Szczygiel [35] also took into account this mechanism to explain the protective behaviour of ZrO_2-base sol-gel coatings deposited on FeCrAl alloys.

In view of the above, it may be confirmed that the same mechanism is occurring in the ZrO_2-Y_2O_3 system assessed in this study, to an even higher degree considering the results obtained by EDX and XRD, where Fe-Zr pairs have been clearly detected. Thus, Fig. 11 shows the potential corrosion mechanism followed by the coated P91 samples, where both coating and diffusion layers are shown, including also the diffusion of the main species involved in the mechanism.

4 Conclusions

This study assessed the protective effect of ZrO_2–3%molY_2O_3 sol-gel coatings on 9Cr-1Mo ferritic-martensitic steel (ASME Grade P91/T91) when working in contact with Solar Salt for CSP applications. To this end, isothermal corrosion tests were performed at 500 °C for 2000 h in order to compare the behaviour of both coated and uncoated P91 samples. Apart from a gravimetric analysis, a microstructural and compositional study was performed on the samples using SEM – EDX and XRD analysis at the end of the tests.

Corrosion results demonstrated the good behaviour of the assessed coating system and its distinct protective properties. The weight-change curve of the coated specimens compared to the uncoated ones reveals the beneficial influence of the coating on corrosion resistance of P91 in contact with molten nitrate salt. After 2000 h of testing, uncoated samples showed a weight increase of 0.3980 mg·cm^{-2}, while the weight gain of the coated samples remained practically unaltered, which indicates the stability of the system throughout the entire test. Regarding the microstructural and compositional study, spallation of oxide scales and corrosion products was observed in the uncoated samples, presenting a multi-layered structure with non-adherent corrosion layers consisting of Fe_2O_3 and Fe_3O_4 in the outer layer and $FeCr_2O_4$ in the inner layer. The microstructural and compositional study performed on the coated samples revealed the maintenance of the coating layer and the presence of a 5.18 μm-thick diffusion layer. This diffusion layer mainly consists of Fe-Zr species, which are well known for reducing the ionic diffusion in the coated system and thus improving its protective properties.

The results reveal the possible suitability of the proposed system as a potential solution to the severe corrosion problems that currently affect industrial tanks and pipes operating in contact with Solar Salt.

Funding Open Access funding provided thanks to the CRUE-CSIC agreement with Springer Nature.

Compliance with ethical standards

Conflict of interest The authors declare no competing interests.

Publisher's note Springer Nature remains neutral with regard to jurisdictional claims in published maps and institutional affiliations.

References

1. Bonk A, Sau S, Uranga N, Henaiz M, Bauer T (2018) Advanced heat transfer fluids for direct molten salt line-focusing CSP plants. Prog Energy Combustion Sci 67:69–87

2. Parrado C, Marzo A, Fuentealba E, Fernández AG (2016) 2050 LCOE improvement using new molten salts for thermal energy storage in CSP plants. Renew Sustain Energy Rev 57:505–514
3. Pintaldi S et al. (2015) A review of thermal energy storage technologies and control approaches for solar cooling. Renew Sustain Energy Rev 41:975–995
4. García-Martín G, Lasanta MI, Encinas-Sánchez V, de Miguel MT, Pérez FJ (2017) Evaluation of corrosion resistance of A516 Steel in a molten nitrate salt mixture using a pilot plant facility for application in CSP plants. Sol Energy Mater Sol Cells 161:226–231
5. Fernández AG, Cortes M, Fuentealba E, Pérez FJ (2015) Corrosion properties of a ternary nitrate/nitrite molten salt in concentrated solar technology. Renew Energy 80:177–183.
6. Dorcheh AS, Durham RN, Galetz MC (2016) Corrosion behaviour of stainless and low-chromium steels and IN625 in molten nitrate salts at 600 °C. Sol Energy Mater Sol Cells 144:109–116
7. Xu Y, Xia T, Wang W, Zhang G, Jia B (2015) Hot corrosion failure mechanism of graphite materials in molten solar salt. Sol Energy Mater Sol Cells 132:260–266
8. Fernández AG, Rey A, Lasanta I, Mato S, Brady MP, Perez FJ (2014) Corrosion of alumina-forming austenitic steel in molten nitrate salts by gravimetric analysis and impedance spectroscopy. Mater Corros 65:267–275
9. Goods SH, Bradshaw RW (2004) Corrosion of stainless steels and carbon steel by molten mixtures of commercial nitrate salts. J Mater Eng Perform 13:78–87
10. Cabet C, Dalle F, Gaganidze E, Henry J, Tanigawa H (2019) Ferritic-martensitic steels for fission and fusion applications. J Nucl Mater 523:510–537. https://doi.org/10.1016/j.jnucmat.2019.05.058
11. Criado M, Sobrados I, Bastidas JM, Sanz J (2015) Steel corrosion in simulated carbonated concrete pore solution its protection using sol-gel coatings. Prog Org Coat 88:228–236
12. Obrtlík K, Celko L, Chráska T, Sulák I, Gejdos P (2017) Effect of alumina-silica-zirconia eutectic ceramic thermal barrier coating on the low cycle fatigue behaviour of cast polycrystalline nickel-based superalloy at 900 °C. Surf Coat Technol 318:374–381
13. Xin D et al. (2019) 'Research status of high corrosion-resistant Zn-Al-Mg coating'. Chin J Eng 41:847–856. https://doi.org/10.13374/J.ISSN2095-9389.2019.07.002
14. Soleimani-Dorcheh A, Galetz MC (2016) Slurry aluminizing: a solution for molten nitrate salt corrosion in concentrated solar power plants. Sol Energy Mater Sol Cells 146:8–15
15. Gurr M, Bau S, Burmeister F, Wirth M, Piedra-González E, Krebser K, Preussner J, Pfeiffer W (2015) Investigation of the corrosion behavior of NiVAl multilayer coatings in hot salt melts. Surf Coat Technol 279:101–111
16. Audigié P, Bizien N, Baraibar I, Rodríguez S, Pastor A, Hernández M, Agüero A (2017) Aluminide slurry coatings for protection of ferritic Steel in molten nitrate corrosion for concentrated solar power technology. AIP Conf Proc 1850:070002
17. Fähsing D, Oskay C, Meißner TM, Galetz MC (2018) Corrosion testing of diffusion-coated steel in molten salt for concentrated solar power tower systems. Surf Coat Technol 354:46–55
18. Gomez-Vidal J, Morton E (2016) Castable cements to prevent corrosion of metals in molten salts. Sol Energy Mater Sol Cells 153:44–51
19. Wang D, Bierwagen GP (2009) Sol-gel coatings on metals for corrosion protection, progess in organic. Coatings 64:327–338
20. Choudhury P, Agrawal DC (2011) Sol–gel derived hydroxyapatite coatings on titanium substrates, surface & coating. Technology 206:360–365
21. Curkovic L, Curkovic HO, Salopek S, Renjo MM, Šegota S (2013) Enhancement of corrosion protection of AISI 304 stainless steel by nanostructured sol–gel TiO2 films. Corros. Sci. 77:176–184
22. Huan Y, Wu K, Li C, Liao H, Debliquy M, Zhang C (2020) 'Micro-nano structured functional coatings deposited by liquid plasma spraying'. J Adv Ceram 9:517–534. https://doi.org/10.1007/S40145-020-0402-9/METRICS
23. Smieszek A, Donesz-Sikorska A, Grzesiak J, Krzak J, Marycz K (2014) 'Biological effects of sol-gel derived ZrO2 and SiO2/ZrO2 coatings on stainless steel surface - In vitro model using mesenchymal stem cells'. J Biomater Appl 29:699–714. https://doi.org/10.1177/0885328214545095
24. Di Maggio R, Fedrizzi L, Rossi S, Scardi P (1996) Dry and wet corrosion behaviour of AISI 304 stainless steel coated by sol–gel ZrO2-CeO2 films. Thin Solid Films 286:127–135
25. Díaz-Parralejo A, Ortiz AL, Caruso R (2010) Effect of sintering temperature on the microstructure and mechanical properties of ZrO2-3 mol%Y2O3 sol–gel films. Ceram Int 36:2281–2286
26. Johnson BY, Edington J, Williams A, O'Keefe MJ (2005) Microstructural characteristics of cerium oxide conversion coatings by various aqueous deposition methods. Mater Charact 54:41–48
27. Amri A, Jiang Z-T, Pryor T, Yin C-Y, Xie Z, Mondinos N (2012) Optical and mechanical characterization of novel cobalt-based metal oxide thin films synthesized using sol–gel dip-coating method. Surf Coat Technol 207:367–374
28. Mimura K, Kato K (2013) Characteristics of barium titanate nanocube ordered assembly thin films fabricated by dip-coating method. Jpn J Appl Phys 52:09KC06
29. Zhou H, Fang J, Chen Y, Yang L, Zhang H, Lu Y, He Y (2016) Internal friction studies on dynamic strain aging in P91 ferritic steel. Mater Sci Eng A 676:361–365
30. Encinas-Sánchez V, Macías-García A, Díaz-Díez MA, Brito P, Cardoso D (2015) Influence of the quality and uniformity of ceramic coatings on corrosion resistance. Ceram Int 41:5138–5146
31. Encinas-Sánchez V, Macías-García A, Díaz-Díez MA, Díaz-Parralejo A (2016) Characterization of sol–gel coatings deposited on a mechanically treated stainless steel by using a simple non-destructive electrical method. J Ceramic Soc Jpn 124:185–191
32. Zhao CY, Wu ZG (2011) Thermal property characterization of a low melting-temperature ternary nitrate salt mixture for thermal energy storage systems. Sol Energy Mater Sol Cells 95:3341–3346
33. Encinas-Sánchez V, Batuecas E, Macías-García A, Mayo C, Díaz R, Pérez FJ (2018) Corrosion resistance of protective coatings against molten nitrate salts for thermal energy storage and their environmental impact in CSP technology. Sol Energy 176:688–697
34. Encinas-Sánchez V, Macías-García A, Pérez FJ (2017) Effect of withdrawal rate on the evolution of optical properties of dip-coated yttria-doped zirconia thin films. Ceram Int 43:13094–13100
35. Carrasco-Amador JP, Díaz-Parralejo A, Macías-García A, Díaz-Díez MA, Olivares-Marín M (2017) Preparation and characterization of $ZrO_2/Y_2O_3/Al_2O_3$-based microstructured multilayer sol–gel coatings. Ceram Int 43:14210–14217
36. Chęcmanowski JG, Szczygiel B (2013) Effect of a ZrO_2 coating deposited by the sol-gel method on the resistance of FeCrAl alloy in high-temperature oxidation conditions. Mater Chem Phys 139:944–952
37. Baron YS, Ruiz A, Navas G (2008) High temperature oxidation resistance of 1.25Cr-0.5Mo wt.% steels by zirconia coating. Surf Coat Technol 202:2616–2622
38. Carling RW, Kramer CM, Bradshaw RW, Nissen DA, Goods SH, Mar RW, Munford JW, Karnowsky MM, Biefeld RN, Norem NJ (1981) Molten nitrate salt technology. Dev NASA STI/Recon Tech Rep N 81:25540
39. Fernández AG, Lasanta MI, Pérez FJ (2012) Molten salt corrosion of stainless steels and low-Cr steel in CSP plants. Oxid Metals 78:329–348
40. Kearney D, Mahoney R (2002) Assessment of a molten heat transfer fluid in a parabolic trough solar field, Solar. Energy Eng 125:170–176

41. Bonk A, Sau S, Uranga N, Hernaiz M, Bauer T (2018) Advanced heat transfer fluids for direct molten salt line-focusing CSP plants. Prog Energy Combust Sci 67:69–87
42. Audigié P, Encinas-Sánchez V, Juez-Lorenzo M, Rodríguez S, Gutiérrez M, Pérez FJ, Agüero A (2018) High temperature molten salt corrosion behavior of aluminide and nickel-aluminide coatings for heat storage in concentrated solar power plants. Surf Coat Technol 349:1148–1157
43. Agüero A, Audigié P, Rodriguez S, Encinas-Sánchez V, de Miguel MT, Pérez FJ (2018) Protective coatings for high temperature molten salt heat storage systems in solar concentration power plants. AIP Conf Proc 2033:090001
44. Kruizenga A, Gill D (2014) Corrosion of iron stainless steels in molten nitrate salt. Energy Procedia 49:878–887
45. Slusser JW, Titcomb JB, Heffelfinger MT, Dunbobbin BR (1985) Corrosion in molten nitrate-nitrite salts. J Metals 37:24–27
46. Sharma P, Kimura H, Inoue A (2008) Magnetic behavior of cosputtered Fe-Zr amorphous thin films exhibiting perpendicular magnetic anisotropy. Phys Rev B 78:134414
47. Czerwinsky F, Szpunar JA (1996) Optimization properties of CeO2 sol-gel coatings for protection of metallic substrates against high temperature oxidation. Thin Solid Films 289: 213–219